© 2014. Published by The Company of Biologists Ltd | Development (2014) 141, 2361 doi:10.1242/dev.112706

CORRECTION

Non-invasive long-term fluorescence live imaging of *Tribolium castaneum* embryos

Frederic Strobl and Ernst H. K. Stelzer

There were errors in the version of *Development* **141**, 2331-2338 that was published on ePress on May 6th, 2014.

In the Results and Discussion, Figs 2 and 3 were incorrectly cited as follows: in the section Characteristics of the EFA-nGFP *Tribolium* line in LSFM, citations to Fig. 3C, 3D, 3E and 3F should have been to Fig. 2C, 2D, 2E and 2F; in the section Serosa scar formation and serosa opening, citations to Fig. 2A and 2B (first paragraph) should have been to Fig. 3A and 3B, and the citation to Fig. 2C (last paragraph) should have been to Fig. 3C.

In the Materials and Methods, lines 13/14 of the Image processing section should have stated: Images that underwent this procedure are marked as maximum projections with image processing (MP).

These errors have been corrected in the full online and print issues.

The authors apologise to readers for these mistakes.

© 2014. Published by The Company of Biologists Ltd | Development (2014) 141, 2331-2338 doi:10.1242/dev.108795

RESEARCH REPORT

TECHNIQUES AND RESOURCES

Non-invasive long-term fluorescence live imaging of *Tribolium castaneum* embryos

Frederic Strobl and Ernst H. K. Stelzer*

ABSTRACT

Insect development has contributed significantly to our understanding of metazoan development. However, most information has been obtained by analyzing a single species, the fruit fly *Drosophila melanogaster*. Embryonic development of the red flour beetle *Tribolium castaneum* differs fundamentally from that of *Drosophila* in aspects such as short-germ development, embryonic leg development, extensive extra-embryonic membrane formation and non-involuted head development. Although *Tribolium* has become the second most important insect model organism, previous live imaging attempts have addressed only specific questions and no long-term live imaging data of *Tribolium* embryogenesis have been available. By combining light sheet-based fluorescence microscopy with a novel mounting method, we achieved complete, continuous and non-invasive fluorescence live imaging of *Tribolium* embryogenesis at high spatiotemporal resolution. The embryos survived the 2-day or longer imaging process, developed into adults and produced fertile progeny. Our data document all morphogenetic processes from the rearrangement of the uniform blastoderm to the onset of regular muscular movement in the same embryo and in four orientations, contributing significantly to the understanding of *Tribolium* development. Furthermore, we created a comprehensive chronological table of *Tribolium* embryogenesis, integrating most previous work and providing a reference for future studies. Based on our observations, we provide evidence that serosa window closure and serosa opening, although deferred by more than 1 day, are linked. All our long-term imaging datasets are available as a resource for the community. *Tribolium* is only the second insect species, after *Drosophila*, for which non-invasive long-term fluorescence live imaging has been achieved.

KEY WORDS: Arthropod development, Coleoptera, *Tribolium castaneum*, Serosa scar, Morphogenesis, Embryogenesis, Light sheet-based fluorescence microscopy, LSFM, DSLM

INTRODUCTION

Research on insect model organisms is an indispensable element in developmental biology (Bodmer and Venkatesh, 1998; Kumar, 2001; Bellen et al., 2010). Although around one million species from the insect order have been described (Patel, 2000), the fruit fly *Drosophila melanogaster* has an almost unchallenged status in the insect developmental biology community. The red flour beetle *Tribolium castaneum* is considered an emerging model organism and has become the second most important insect species after *Drosophila* (Klingler, 2004; Schröder et al., 2008; Brown et al., 2009). In contrast to *Drosophila*, *Tribolium* exhibits short-germ development, in which segments are added sequentially to the posterior growth zone (Liu and Kaufman, 2005; Roth and Hartenstein, 2008; Schröder et al., 2008), and embryonic leg development (Grossmann and Prpic, 2012). Other aspects of *Tribolium* development are also considered representative for the insect order, such as extensive extra-embryonic membrane formation (Handel et al., 2005; Panfilio, 2008; Benton et al., 2013; Panfilio et al., 2013) and non-involuted head development (Peel, 2008; Schinko et al., 2008; Posnien and Bucher, 2010). On the methodology side, some molecular biological tools have a higher potency in *Tribolium* than in *Drosophila*, and since the *Tribolium* genome was recently sequenced (Richards et al., 2008), RNA interference (Bucher et al., 2002; Tomoyasu and Denell, 2004; Tomoyasu et al., 2008) has become a very powerful technique for the analysis of gene functions.

A recent approach to study *Tribolium* development has been fluorescence live imaging. First reports have described blastoderm formation, gastrulation, the beginning of germband elongation and dorsal closure by imaging the transgenic EFA-nGFP line or transiently labeled embryos by confocal microscopy (El-Sherif et al., 2012; Sarrazin et al., 2012; Benton et al., 2013; Panfilio et al., 2013). However, no long-term fluorescence live imaging of *Tribolium* embryogenesis has been available until now.

Recently, light sheet-based fluorescence microscopy (LSFM) has emerged as the alternative to confocal fluorescence microscopy and thus constitutes one of the most valuable novel tools in developmental biology (Hell et al., 1994; Stelzer and Lindek, 1994; Huisken et al., 2004; Keller et al., 2008). The complete morphogenesis of *Drosophila* has already been imaged with great success (Keller et al., 2010). In contrast to an epifluorescence arrangement, LSFM uses at least two independently operated lenses. The lenses used in the excitation of the fluorophores are arranged at an angle of 90° relative to those used for the detection of the three-dimensional fluorophore density distribution. Special optical arrangements illuminate only a thin planar section centered on the focal planes of the detection lenses. Hence, true optical sectioning as well as no phototoxic damage and no photobleaching outside a small volume close to the focal plane are intrinsic properties of LSFM. The energy required to excite the fluorophores while recording a three-dimensional stack of images is reduced by two to four orders of magnitude relative to conventional, confocal and two-photon fluorescence microscopy. Since modern cameras are used to record millions of pixels in parallel, tens to hundreds of images with subcellular resolution can be recorded within a few seconds (Keller and Stelzer, 2010).

Here, we describe a novel mounting method for non-invasive long-term fluorescence live imaging of *Tribolium* embryos in LSFM. We show all morphogenetic processes from the rearrangement of the uniform blastoderm to the onset of regular muscular movement

Physical Biology/Physikalische Biologie (IZN, FB 15), Buchmann Institute for Molecular Life Sciences (BMLS), Cluster of Excellence Frankfurt – Macromolecular Complexes (CEF – MC), Goethe University – Frankfurt am Main (Campus Riedberg), Max-von-Laue-Straße 15, Frankfurt am Main D-60348, Germany.

*Author for correspondence (ernst.stelzer@physikalischebiologie.de)

Received 6 February 2014; Accepted 28 March 2014

Development (2014) 141, 2331-2338 doi:10.1242/dev.108795

continuously in the same embryo and in four orientations and provide a comprehensive chronological description of *Tribolium* embryogenesis. As an example of the quality and applicability of our data, we provide evidence that serosa window closure and serosa opening, two processes that occur more than 1 day apart, are functionally linked via a previously undescribed structure, the serosa scar. All of our long-term imaging datasets are available as a resource for the community.

RESULTS AND DISCUSSION

A novel mounting method for *Tribolium* embryos in LSFM

The development of *Tribolium* embryos stops after a few hours when they are embedded in agarose columns, a mounting method that, by contrast, works well with *Drosophila* embryos (Keller et al., 2011). We assume that this is caused by mechanical constraints, reduced gas exchange or a combination of both. Therefore, we developed a novel mounting method in which only a minor fraction of the egg surface is attached to the top of an agarose hemisphere, while the major fraction of the egg surface is exposed to the buffer (supplementary material Fig. S1A). This method allowed us to image *Tribolium* for more than 2 days by LSFM (supplementary material Fig. S1B) until the onset of regular muscular movement (supplementary material Fig. S1C).

Non-invasive long-term fluorescence live imaging of *Tribolium* embryos

With the novel mounting method, we obtained three non-invasive long-term fluorescence live imaging datasets of three embryos from the EFA-nGFP transgenic line (Sarrazin et al., 2012). All three embryos were able to hatch into larvae (supplementary material Fig. S1D), developed into adults that showed no abnormalities, produced healthy and fertile progeny and were still alive at the end of the study. Therefore, we infer that our data were obtained in an as close-to-natural fashion as possible, establishing quality standards that have to be met by future studies.

Our data allow us to summarize nearly the complete course of *Tribolium* embryogenesis from the rearrangement of the uniform blastoderm to the onset of regular muscular movement in a dynamic fashion, including four embryogenesis events that are considered fundamental throughout the insect class – gastrulation, germband elongation, germband retraction and dorsal closure (Fig. 1; supplementary material Movie 1). Furthermore, we created a chronological description of *Tribolium* embryogenesis that links our observations with the current literature (Table 1).

Summary of *Tribolium* morphogenesis

After blastoderm formation, gastrulation begins with the rearrangement of the uniform blastoderm, which differentiates into the serosa and the embryonic rudiment. The serosa migrates over the posterior pole and grows over the embryonic rudiment, initiating the invagination process. The embryonic rudiment condenses and sinks into the yolk (Fig. 1A). Once the serosa window closes, the embryonic rudiment is released into the interior of the serosa, differentiating into the germband, thereby initiating germband elongation. Segments are now added sequentially to the posterior growth zone. The germband tips curl around both poles, migrating dorsally towards each other. Segmentation becomes more prominent in the thoracic region and leg development begins (Fig. 1B). Germband retraction is accompanied by extensive broadening and the germband flanks bend laterally towards the dorsal side. Legs reach their maximum length while pleuropodia develop at the first abdominal segment and the head becomes clearly separated from the thorax (Fig. 1C). When the germband has retracted completely, dorsal closure begins. After opening, the serosa first migrates over the anterior, then over the posterior pole and turns inside-out on the dorsal side, forming the dorsal organ. Finally, the dorsal organ is incorporated into the dorsal center when both germband flanks close (Fig. 1D). Shortly after dorsal closure, regular muscular movement sets in.

Characteristics of the EFA-nGFP *Tribolium* line in LSFM

In contrast to *Drosophila*, *Tribolium* develops appendices during embryogenesis. We investigated how far these structures can be visualized with LSFM. During dorsal closure, the head performs a ~45° turn from an anterior to an anterior-ventral position (Fig. 2A). On the single planes, we were able to resolve and follow structures such as the labial palps and the mandibles over time (Fig. 2B; supplementary material Movie 2). Even deep within the embryo, we could still resolve the trachea as well as the esophagus with its butterfly-shaped inner lumen above the subesophageal ganglion (Fig. 2C; supplementary material Movie 2).

An important issue with long-term fluorescence imaging is photobleaching. If datasets were recorded with an imaging interval of 00:06 h, moderate photobleaching occurred, whereas with an interval of 00:30 h photobleaching was barely visible (supplementary material Fig. S2), maintaining a signal-to-noise ratio that was sufficient to perform volume renderings of the complete dataset (supplementary material Movie 3). Volume rendering visualized certain structures more efficiently; for example, median groove folding during gastrulation or embryonic leg development (Fig. 2D). Furthermore, our LSFM setup was sufficiently sensitive to observe cell proliferation in the EFA-nGFP line. During gastrulation, dividing nuclei could be detected as light gray clouds over a dark gray background (Fig. 2E), and, even beyond gastrulation, sites of massive proliferation could be determined; for example, at the outer rims of the head lobes during germband elongation (Fig. 2F).

Serosa scar formation and serosa opening

As an example of the practical application of our data, we characterized a previously undescribed transient structure that emerges and vanishes again in between serosa differentiation and internalization. After serosa window closure, in many, but not all, instances, the germband rotated slightly around the anterior-posterior axis. This rotation revealed an anterior-ventral cell cluster on the serosa, which we term the serosa scar (Fig. 3A; supplementary material Movie 4). For approximately one-third of embryogenesis, the serosa scar remained quiescent in the same location. Shortly before dorsal closure, the serosa scar was pulled apart in a circular fashion. The pulling redirected dorsally, which led to elimination of the space between the serosa and the germband. This was followed by the migration of the serosa over the anterior pole (Fig. 3B; supplementary material Movie 5).

The cell movement pattern suggests that the serosa scar is established at the end of gastrulation as a predetermined point for the formation of an anterior-ventral serosa opening during dorsal closure once pulling at the dorsal side begins. This view is supported by evidence that the space between the serosa and the germband is eliminated, which indicates a subsequent liquid outflow through the newly formed serosa opening.

Spatiotemporally separated and functionally distinct morphogenetic processes, such as serosa window closure (Handel et al., 2000; Benton et al., 2013) and serosa opening (van der Zee et al., 2005; Panfilio et al., 2013), have been described previously, but were not related to preceding and subsequent processes. Therefore, those investigations had not been able to demonstrate a higher order

Development (2014) 141, 2331-2338 doi:10.1242/dev.108795

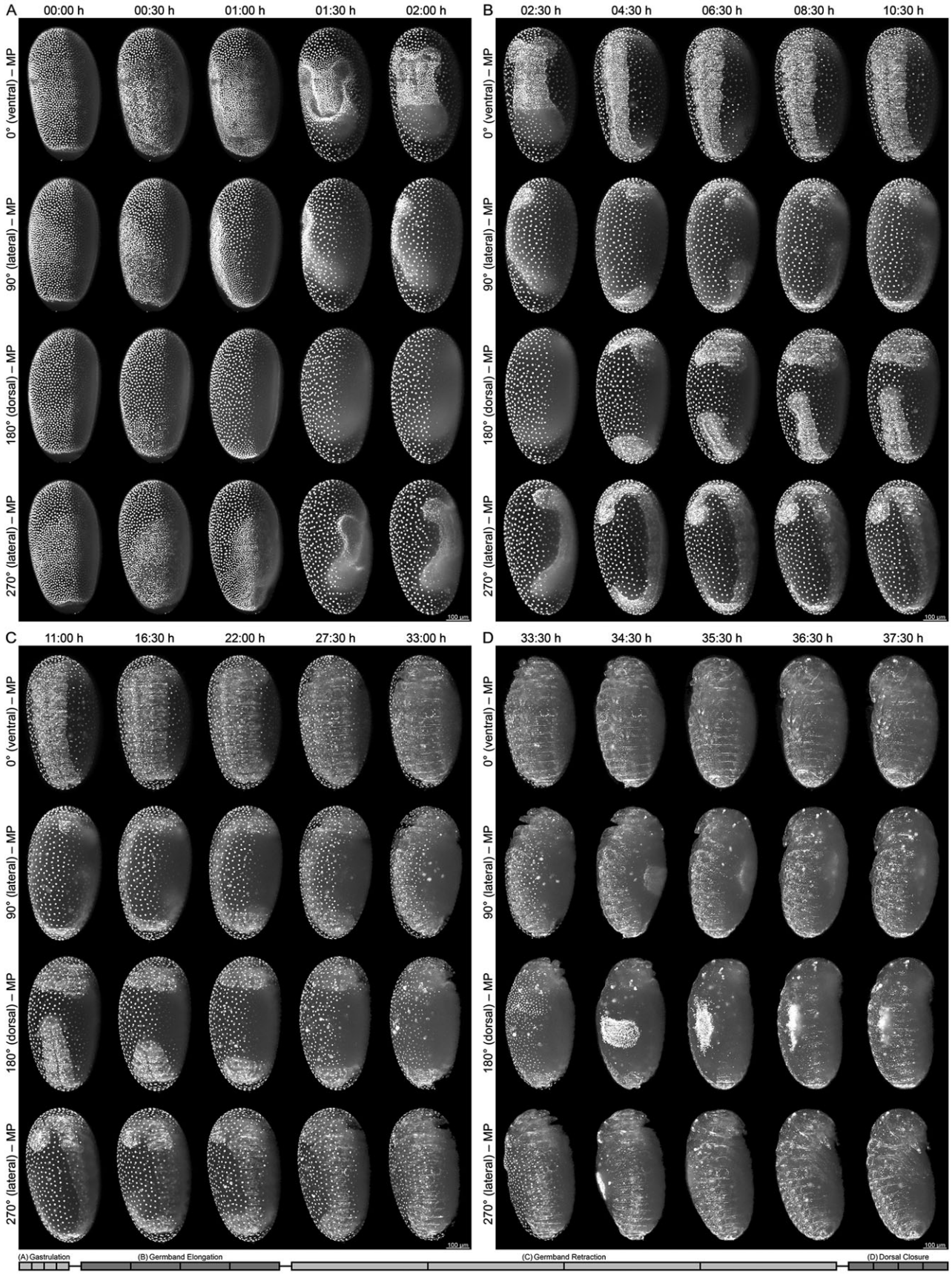

Fig. 1. Overview of *Tribolium* embryogenesis. The four embryogenesis events of (A) gastrulation, (B) germband elongation, (C) germband retraction and (D) dorsal closure of *Tribolium* are shown in four orientations over a period of 37:30 h. The progression bar at the bottom indicates the temporal frame of the images (each black bar represents one time point). MP, maximum projection with image processing.

Development (2014) 141, 2331-2338 doi:10.1242/dev.108795

Table 1. Chronological description of *Tribolium* embryogenesis

Figure and time	Developmental process
Before imaging	• The twelfth and last synchronous blastodermal proliferation cycle finishes (Handel et al., 2000, 2005; Benton et al., 2013) o giving rise to the uniform blastoderm (Brown et al., 1994; Handel et al., 2000, 2005; Benton et al., 2013)
	End of blastoderm formation and beginning of gastrulation
1A – 00:00 h	• The uniform blastoderm rearranges into the differentiated blastoderm (Brown et al., 1994; Handel et al., 2000; van der Zee et al., 2005; Benton et al., 2013) o spreading into a dorsally tilted anterior cap (Handel et al., 2000) – representing the future extra-embryonic tissue o clustering into a ventrally tilted posterior cap (Handel et al., 2000; El-Sherif et al., 2012) – representing the future germband • The posterior pole flattens ventrally and forms a plate (Handel et al., 2000) o usually accompanied by a retraction of the posterior pole from the vitelline membrane (Benton et al., 2013)
1A – 00:30 h	• The thirteenth asynchronous proliferation cycle finishes laterally (Handel et al., 2000, 2005; El-Sherif et al., 2012; Benton et al., 2013) o forming the serosa consisting of large and widespread nuclei (Brown et al., 1994; Handel et al., 2000; van der Zee et al., 2005; Benton et al., 2013) o forming the median ventral stripe consisting of large and clustered nuclei (Handel et al., 2000, 2005) o forming the embryonic rudiment flanks consisting of small and condensed nuclei (Brown et al., 1994; Handel et al., 2000; van der Zee et al., 2005; Benton et al., 2013) • The posterior pole invaginates (Handel et al., 2000; Handel et al., 2005; Benton et al., 2013) o turning the plate at the posterior pole into the primitive pit (Brown et al., 1994; Handel et al., 2000; Handel et al., 2005; van der Zee et al., 2005; Benton et al., 2013)
1A – 01:00 h	• The median ventral stripe finishes the thirteenth proliferation cycle (Handel et al., 2005) o turning into the middle plate (Handel et al., 2000) o joining both embryonic rudiment flanks • The serosa extends to the ventral center around the lateral sides and towards the posterior pole (Brown et al., 1994; Handel et al., 2000; van der Zee et al., 2005; Benton et al., 2013) o condensing the embryonic rudiment (Brown et al., 1994; Handel et al., 2000, 2005; El-Sherif et al., 2012; Sarrazin et al., 2012; Benton et al., 2013) o overgrowing the primitive pit (Brown et al., 1994; Handel et al., 2000; Benton et al., 2013) – forming the posterior amniotic fold (Handel et al., 2000, 2005; van der Zee et al., 2005; Sarrazin et al., 2012; Benton et al., 2013)
1A – 01:30 h	• The embryonic rudiment sinks into the yolk (Brown et al., 1994; Handel et al., 2005; Sarrazin et al., 2012; Benton et al., 2013) • The middle plate folds into the median groove (Brown et al., 1994; Handel et al., 2000, 2005) • The dorsal serosa rotates over the posterior pole (Handel et al., 2000; Benton et al., 2013) • The posterior amniotic fold internalizes the embryonic rudiment (Brown et al., 1994; Handel et al., 2005; Sarrazin et al., 2012; Benton et al., 2013) o rotating the posterior and posterior-lateral amnion inward (Handel et al., 2000; Benton et al., 2013) o forming the yolk sac fold (Handel et al., 2000; Benton et al., 2013) • The anterior amniotic fold elevates (Brown et al., 1994; Handel et al., 2000; van der Zee et al., 2005; Benton et al., 2013) o involuting head lobes (Brown et al., 1994) o joining subsequently with the posterior amniotic fold (Handel et al., 2000; van der Zee et al., 2005) – resulting in a combined horseshoe-shaped amniotic fold (Handel et al., 2000; van der Zee et al., 2005; Benton et al., 2013)
1A – 02:00 h	• The combined amniotic fold gives rise to the serosa window (Handel et al., 2000; van der Zee et al., 2005; Benton et al., 2013) o changing the horseshoe-shaped amniotic fold into an oval amniotic fold (Benton et al., 2013) o bearing slight notches close to the head lobe anlagen o rotating the anterior and anterior-lateral amnion inward (Handel et al., 2000) – allowing the future head lobes to extend below the serosa to the anterior pole (van der Zee et al., 2005)
	End of gastrulation and beginning of germband elongation
1B – 02:30 h	• The serosa window closes (Handel et al., 2000; van der Zee et al., 2005; Kittelmann et al., 2013; Sarrazin et al., 2012; Benton et al., 2013) o separating the serosa from the amnion (Handel et al., 2000; Benton et al., 2013) – releasing the embryonic rudiment with the affiliated amnion into the interior of the serosa (van der Zee et al., 2005) • The embryonic rudiment differentiates into the germband (Brown et al., 1994; Handel et al., 2000; Benton et al., 2013) o forming the posterior growth zone (Brown et al., 1994; Handel et al., 2005) – initiating germband elongation (Brown et al., 1994; van der Zee et al., 2005; Sarrazin et al., 2012; Benton et al., 2013) • The yolk sac fold retracts (Handel et al., 2000; Benton et al., 2013)
1B – 04:30 h	• The yolk sac fold levels out (Handel et al., 2000) o allowing the posterior growth zone to reach the posterior pole (Brown et al., 1994; Handel et al., 2000; Benton et al., 2013) o leading to a superficial germband that spans over the complete egg length (Brown et al., 1994; Handel et al., 2000) • The head lobes curl around the anterior pole (Brown et al., 1994; Benton et al., 2013) o extending dorsally towards the posterior pole • The posterior growth zone curls around the posterior pole (Brown et al., 1994; Benton et al., 2013) o extending dorsally towards the anterior pole (Benton et al., 2013) – resulting in an approaching dorsal movement both germband tips, the head lobes and the posterior growth zone
1B – 06:30 h	• The head lobes stop migrating dorsally o leading to a proliferation anterior median region (Kittelmann et al., 2013) – fusing the head lobes medially (Kittelmann et al., 2013)

Continued

Development (2014) 141, 2331-2338 doi:10.1242/dev.108795

Table 1. Continued

Figure and time	Developmental process
	• The mandibular and maxillary segment outlines become visible (Brown et al., 1994; Handel et al., 2005)
	• The appendage buds become visible (Brown et al., 1994; Handel et al., 2005)
	• The thorax exhibits a more prominent segmentation (Brown et al., 1994)
1B – 08:30 h	• The thoracic segments initiate leg development
	○ pushing the germband slightly into the yolk
	• The abdomen exhibits a more prominent segmentation
	• The posterior growth zone spans half of the egg length
1B – 10:30 h	• The posterior growth zone spans slightly more than half of the egg length
	○ allowing the germband to reach the maximal length (Brown et al., 1994; van der Zee et al., 2005)
	○ reaching the extended germband stage (Brown et al., 1994)
	End of germband elongation and beginning of germband retraction
1C – 11:00 h	• The germband begins with retraction
	○ exhibiting massive proliferation at the posterior growth zone
1C – 16:30 h	• The germband retracts posteriorly to one-third of the egg length
	○ broadening parallel to two-thirds of the egg width
	• At the tip of the posterior growth zone, the hindgut is formed
1C – 22:00 h	• The germband retracts posteriorly to one-fifth of the egg length
	○ broadening parallel to three-quarters of the egg width
1C – 27:30 h	• The head becomes clearly separated from the thorax
	• The germband retracts posteriorly nearly completely
	○ broadening parallel to the full egg width
	• The first abdominal segment develops pleuropodia
1C – 33:00 h	• The germband flips posteriorly into the posterior pole
	○ allowing the germband to reach minimal length (Brown et al., 1994)
	○ broadening even further (Brown et al., 1994; van der Zee et al., 2005)
	– leading to a lateral bending and the dorsal growth of the germband flanks (Brown et al., 1994; van der Zee et al., 2005)
	• The serosa is pulled to the dorsal center
	○ stretching the serosa slightly
	End of germband retraction and beginning of dorsal closure
1D – 33:30 h	• The serosa opens ventrally
	○ initiating serosa withdrawal (Panfilio et al., 2013)
	○ allowing the serosa to migrate over the anterior pole
1D – 34:30 h	• The serosa clusters at the dorsal center of the embryo (Panfilio et al., 2013)
	○ allowing the serosa to migrate over the posterior pole
	– folding over itself (Panfilio et al., 2013)
	– leading to an inside-out turning of the serosa
	○ compacting strongly (Panfilio et al., 2013)
	– reducing the serosa surface area (Panfilio et al., 2013)
	– forming the dorsal organ (van der Zee et al., 2005; Panfilio et al., 2013)
1D – 35:30 h	• The head starts turning from an anterior to an anterior-ventral orientation
	• The germband flanks extend toward the midline (Panfilio et al., 2013)
	• The dorsal organ elongates anterior-posteriorly (Panfilio et al., 2013)
	○ turning the embryo from a dorsally curled position to a ventrally curled position
1D – 36:30 h	• The head has reached the anterior-ventral orientation
	• The dorsal organ sinks into the yolk (van der Zee et al., 2005; Panfilio et al., 2013)
1D – 37:30 h	• The dorsal organ becomes completely internalized
	• The germband flanks begin epidermal zippering (Panfilio et al., 2013)
	○ initiating midline closure (Panfilio et al., 2013)
	○ leaving the dorsal seam behind (Panfilio et al., 2013)
	End of dorsal closure
Beyond imaging	• The germband flanks finish epidermal zippering (Panfilio et al., 2013)
	○ the dorsal seam closes completely (Panfilio et al., 2013)
	• The surface exhibits extensive cell proliferation
	• The embryo exhibits regular muscular movement

We only describe processes for which our data provide evidence. Indentions show associated processes. If applicable, processes are referenced. The references include the majority of current publications, in particular all publications that provide fluorescence live imaging data. We use the original terms suggested in these publications. Please note that some morphogenetic processes can only be seen properly in the supplementary material movies; for example, leg development and serosa stretching.

dynamics of embryogenesis, such as the functional link between serosa window closure and serosa opening that we describe here (Fig. 3C). This example illustrates the importance of non-invasive long-term fluorescence live imaging.

Perspectives

We anticipate that LSFM will become a powerful tool in the analysis of fluorescently labeled transgenic *Tribolium* lines as well as mutants or embryos in which genes have been knocked

Development (2014) 141, 2331-2338 doi:10.1242/dev.108795

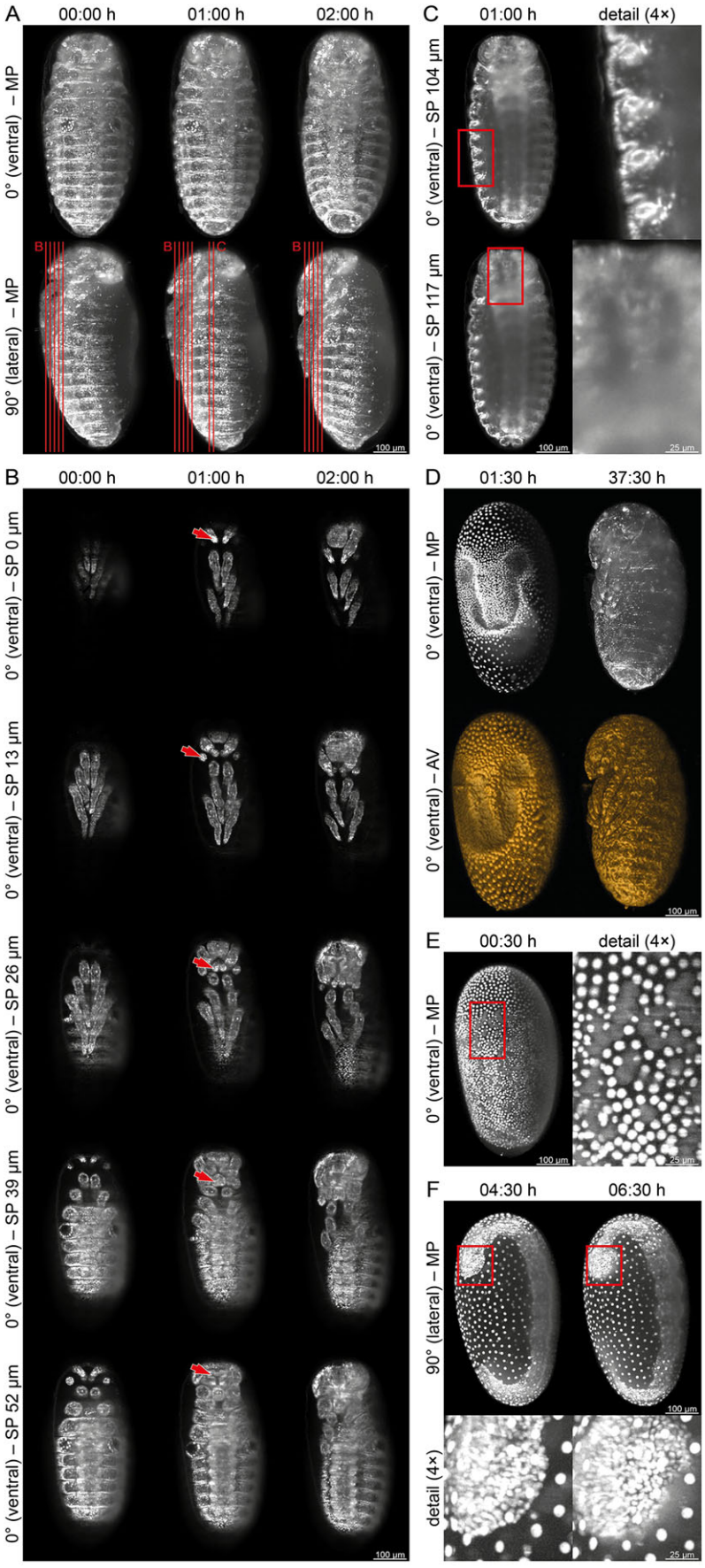

Fig. 2. Characteristics of the EFA-nGFP *Tribolium* line in LSFM. (A) Head movement during dorsal closure. The head turns ~45° from an anterior to an anterior-ventral position during dorsal closure. Lines indicate single planes shown in B and C. (B) Ventral optical sectioning during dorsal closure shows head appendices. The first single plane with moderate signal was defined as 0 µm. Because of the head turning, ventrally recorded single planes show details of head development along different head orientations. Arrows mark the antenna at 0 µm, the maxillary palp tip at 13 µm, the labial palps at 26 µm, the labium at 39 µm and the mandibles with the typical Y-shape in between at 52 µm. (C) Ventral optical sectioning during dorsal closure shows structures deep within the embryo. The first single plane with moderate signal was defined as 0 µm. The boxed regions are magnified (4×) to the right. At 104 µm, the tracheae are visible. At 117 µm, the esophagus is cut sagittal, revealing its butterfly-shaped inner lumen. (D) Maximal projections compared with volume rendering. Some structures are better visualized on the volume renderings; for example, the median groove during gastrulation at 01:30 h and the legs during dorsal closure at 37:30 h. (E) Cell proliferation during gastrulation. The boxed region is magnified (4×) to the right. With LSFM, it is possible to visualize cell proliferation during early gastrulation, as dividing cells form light gray 'clouds' above a dark gray background. (F) Cell proliferation beyond gastrulation. The boxed regions are magnified (4×) beneath. Beyond gastrulation, LSFM can still visualize sites of massive cell proliferation, as shown here for the outer rim of the head lobes during germband elongation. MP, maximum projection with image processing; SP, single plane; AV, Amira-based volume rendering.

Development (2014) 141, 2331-2338 doi:10.1242/dev.108795

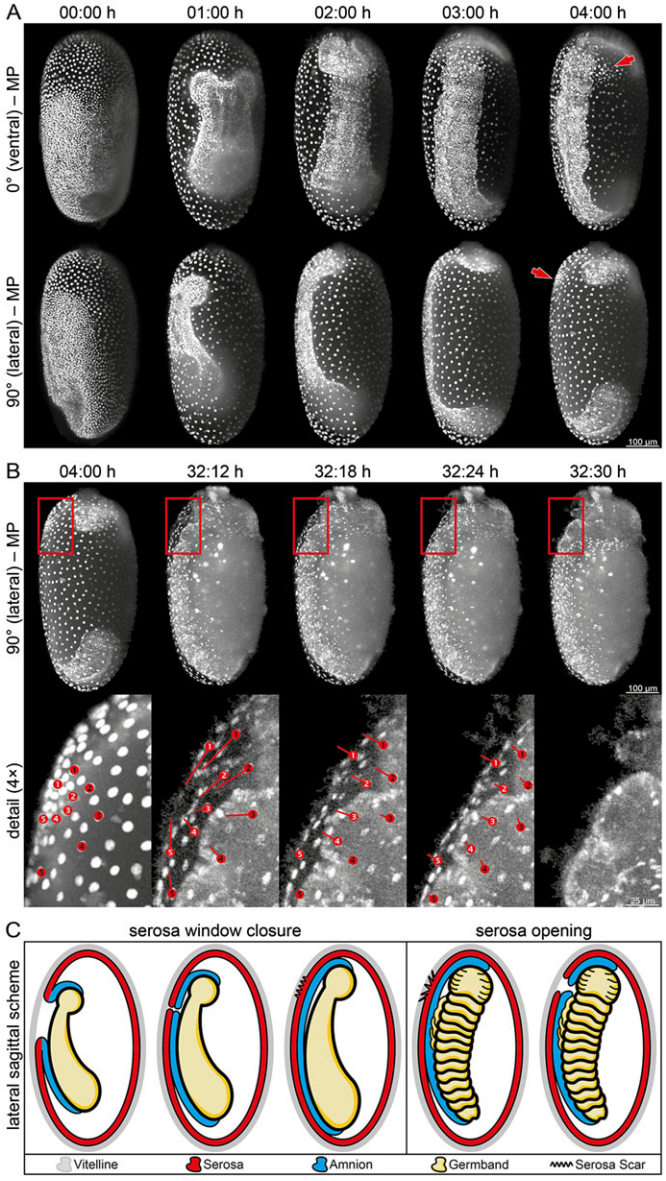

Fig. 3. Serosa scar formation and serosa opening. (A) Serosa window closure and serosa scar formation. During gastrulation, the serosa window emerges and subsequently closes at the anterior-ventral side of the embryo. Then, the germband rotates inside the serosa, exposing a cell cluster at the location where the serosa window closed termed the serosa scar (arrows). (B) Serosa scar quiescence and serosa opening. The boxed regions are magnified (4×) beneath. To illustrate serosa movement, ten nuclei were tracked over time, five in close (white numbers) and five in distal (black numbers) proximity to the center of the serosa scar. Upon serosa window closure, the serosa scar remains quiescent for more than 1 day before being pulled apart in a circular fashion. Then, the migration pattern changes as the nuclei migrate dorsally, eliminating the space between the serosa and the germband. (C) Scheme of serosa window closure, serosa scar formation and serosa opening. During gastrulation, the serosa is separated from the amnion/germband as the serosa window closes and the serosa scar is left behind in the location where the window closed. While embryogenesis proceeds, the serosa scar remains quiescent as the germband undergoes elongation and retraction. Shortly before dorsal closure, the serosa scar is pulled apart, the serosa opening is created and the space between serosa and germband is eliminated. MP, maximum projection with image processing.

down, especially in terms of the development of the head, legs and extra-embryonic membranes, in which *Tribolium* differs significantly from *Drosophila*.

With this work, the complete embryogenesis of a second insect species is now documented, which is an important step for comparative studies. We intend to investigate which other morphogenetic concepts exist besides the *Drosophila* paradigm and how they are executed, identifying fundamental principles as well as specialized alterations and thereby providing insights in the fields of developmental, cell and evolutionary biology.

MATERIALS AND METHODS

Tribolium rearing and embryo collection

The *Tribolium castaneum* (Herbst) Vermillion White EFA-nGFP transgenic line was used (Sarrazin et al., 2012). Rearing and embryo collection were performed as described previously (Brown et al., 2009); parameters are provided in supplementary material Table S1.

Mounting

Simultaneous dechorionation of 10-15 embryos was performed as described previously (Benton et al., 2013). An embryo that exhibited reasonable fluorescence emission under a SteREO Discovery.V8 microscope (Carl Zeiss) with filter set 38 (Carl Zeiss) was picked with a small paint brush. A stainless steel pipe with an external diameter of 3 mm and an internal diameter of 1 mm (#R00306, Sawade Edelstahlrohre, Gottmadingen, Germany) was held vertically and filled with agarose from the top until a hemisphere formed and polymerized at the bottom end of the pipe. The hemisphere was then dipped into liquid agarose in order to apply a thin film that was used to mount the dechorionated embryo with the anterior side to the top of the hemisphere. Finally, 2 µl agarose were added around the gap between the embryo and agarose hemisphere for additional stability (supplementary material Fig. S1). Parameters are provided in supplementary material Table S1.

Microscopy

We used an advanced variant of LSFM termed monolithic digital scanned laser light sheet-based fluorescence microscopy (mDSLM), which is based on DSLM (Keller and Stelzer, 2010). Parameters are provided in supplementary material Table S1. Imaging started immediately after the embryo was inserted into the sample chamber.

Embryo retrieval

When regular muscular movement could be detected (supplementary material Fig. S1C) imaging was stopped. The sample chamber was slowly drained and the agarose hemisphere with the embryo still mounted on top was retrieved and transferred to an object holder. The embryo was dried for 5 min at 35°C, then transferred to a moistening chamber and further incubated at 35°C. After hatching, the larva was transferred to a small glass tube and cultivated as stated above. After the larva had developed into an adult, it was provided with a mating partner. After an appropriate time, progeny production was checked.

Image processing

Image processing was performed with Mathematica (Wolfram). Single planes (SP) were used to calculate the maximum projections. With those projections, two processing steps were performed. (1) Background correction (BC). A brightness threshold was applied that distinguishes the specimen from the background. The background was used to calculate the mean image background and then set to zero. Then, the mean image background was subtracted from the whole image. This led to an overall intensity decrease. (2) Mean transform (MT). For the desired series of images, the brightest and the dimmest images were selected and the mean intensity was calculated. For the desired series, the image closest to that intensity was determined and designated the reference image. All images were normalized to match the intensity of the reference image. This included both increase and decrease of intensities (supplementary material Fig. S3). Images that underwent this procedure are marked as maximum projections with image processing (MP). If necessary, images underwent equal brightness adjustment. Further details of image processing can be provided upon request. Images were cropped to

Development (2014) 141, 2331-2338 doi:10.1242/dev.108795

600×1000 pixels (XD×YD, supplementary material Table S1), maintaining the original line and pixel pitches used during the imaging recording process. Cell tracking in Fig. 3B was performed manually. Amira (FEI Visualization Science Group, Düsseldorf, Germany) was used for volume rendering (AV) in Fig. 2D and supplementary material Movie 3. Meta information about the three long-term imaging datasets is provided in supplementary material Table S1 (the original datasets, associated figures and movies in full quality are available at www.physikalischebiologie.de/bugcube).

Acknowledgements

We thank Andrew Peel and Michalis Averof for the *Tribolium* EFA-nGFP line; the Goethe University workshop for custom hardware; Alexander Schmitz for help with the Mathematica-based image processing; Daniel von Wangenheim for help with the generation of the movies and Amira-based volume rendering; and Isabell Smyrek, Christian Pohl, Anna Gilles and Michalis Averof for comments on the manuscript.

Competing interests

The authors declare no competing financial interests.

Author contributions

F.S. and E.H.K.S. conceived the research and wrote the publication. F.S. performed the experiments.

Funding

This work was supported by the Deutsche Forschungsgemeinschaft (DFG)-funded Cluster of Excellence 'Macromolecular Complexes' [CEF, EXC 115].

Supplementary material

Supplementary material available online at
http://dev.biologists.org/lookup/suppl/doi:10.1242/dev.108795/-/DC1

References

Bellen, H. J., Tong, C. and Tsuda, H. (2010). 100 years of Drosophila research and its impact on vertebrate neuroscience: a history lesson for the future. *Nat. Rev. Neurosci.* **11**, 514-522.

Benton, M. A., Akam, M. and Pavlopoulos, A. (2013). Cell and tissue dynamics during Tribolium embryogenesis revealed by versatile fluorescence labeling approaches. *Development* **140**, 3210-3220.

Bodmer, R. and Venkatesh, T. V. (1998). Heart development in Drosophila and vertebrates: conservation of molecular mechanisms. *Dev. Genet.* **22**, 181-186.

Brown, S. J., Parrish, J. K., Denell, R. E. and Beeman, R. W. (1994). Genetic control of early embryogenesis in the red flour beetle, Tribolium castaneum. *Am. Zoologist* **34**, 343-352.

Brown, S. J., Shippy, T. D., Miller, S., Bolognesi, R., Beeman, R. W., Lorenzen, M. D., Bucher, G., Wimmer, E. A. and Klingler, M. (2009). The red flour beetle, Tribolium castaneum (Coleoptera): a model for studies of development and pest biology. *Cold Spring Harb. Protoc.* **2009**, ppdb emo126.

Bucher, G., Scholten, J. and Klingler, M. (2002). Parental RNAi in Tribolium (Coleoptera). *Curr. Biol.* **12**, R85-R86.

El-Sherif, E., Averof, M. and Brown, S. J. (2012). A segmentation clock operating in blastoderm and germband stages of Tribolium development. *Development* **139**, 4341-4346.

Grossmann, D. and Prpic, N.-M. (2012). Egfr signaling regulates distal as well as medial fate in the embryonic leg of Tribolium castaneum. *Dev. Biol.* **370**, 264-272.

Handel, K., Grünfelder, C. G., Roth, S. and Sander, K. (2000). Tribolium embryogenesis: a SEM study of cell shapes and movements from blastoderm to serosal closure. *Dev. Genes. Evol.* **210**, 167-179.

Handel, K., Basal, A., Fan, X. and Roth, S. (2005). Tribolium castaneum twist: gastrulation and mesoderm formation in a short-germ beetle. *Dev. Genes. Evol.* **215**, 13-31.

Hell, S. W., Stelzer, E. H. K., Lindek, S. and Cremer, C. (1994). Confocal microscopy with an increased detection aperture: type-B 4Pi confocal microscopy. *Opt. Lett.* **19**, 222.

Huisken, J., Swoger, J., Del Bene, F., Wittbrodt, J. and Stelzer, E. H. K. (2004). Optical sectioning deep inside live embryos by selective plane illumination microscopy. *Science* **305**, 1007-1009.

Keller, P. J. and Stelzer, E. H. K. (2010). Digital scanned laser light sheet fluorescence microscopy. *Cold Spring Harb. Protoc.* **2010**, ppdb.top78.

Keller, P. J., Schmidt, A. D., Wittbrodt, J. and Stelzer, E. H. K. (2008). Reconstruction of zebrafish early embryonic development by scanned light sheet microscopy. *Science* **322**, 1065-1069.

Keller, P. J., Schmidt, A. D., Santella, A., Khairy, K., Bao, Z., Wittbrodt, J. and Stelzer, E. H. K. (2010). Fast, high-contrast imaging of animal development with scanned light sheet-based structured-illumination microscopy. *Nat. Methods* **7**, 637-642.

Keller, P. J., Schmidt, A. D., Wittbrodt, J. and Stelzer, E. H. K. (2011). Digital scanned laser light-sheet fluorescence microscopy (DSLM) of zebrafish and Drosophila embryonic development. *Cold Spring Harb. Protoc.* **2011**, 1235-1243.

Kittelmann, S., Ulrich, J., Posnien, N. and Bucher, G. (2013). Changes in anterior head patterning underlie the evolution of long germ embryogenesis. *Dev. Biol.* **374**, 174-184.

Klingler, M. (2004). Tribolium. *Curr. Biol.* **14**, R639-R640.

Kumar, J. P. (2001). Signalling pathways in Drosophila and vertebrate retinal development. *Nat. Rev. Genet.* **2**, 846-857.

Liu, P. Z. and Kaufman, T. C. (2005). Short and long germ segmentation: unanswered questions in the evolution of a developmental mode. *Evol. Dev.* **7**, 629-646.

Panfilio, K. A. (2008). Extraembryonic development in insects and the acrobatics of blastokinesis. *Dev. Biol.* **313**, 471-491.

Panfilio, K. A., Oberhofer, G. and Roth, S. (2013). High plasticity in epithelial morphogenesis during insect dorsal closure. *Biol. Open* **2**, 1108-1118.

Patel, N. H. (2000). It's a bug's life. *Proc. Natl. Acad. Sci. U.S.A.* **97**, 4442-4444.

Peel, A. D. (2008). The evolution of developmental gene networks: lessons from comparative studies on holometabolous insects. *Philos. Trans. R. Soc. Lond. B Biol. Sci.* **363**, 1539-1547.

Posnien, N. and Bucher, G. (2010). Formation of the insect head involves lateral contribution of the intercalary segment, which depends on Tc-labial function. *Dev. Biol.* **338**, 107-116.

Richards, S., Gibbs, R. A., Weinstock, G. M., Brown, S. J., Denell, R., Beeman, R. W., Gibbs, R., Bucher, G., Friedrich, M., Grimmelikhuijzen, C. J. et al. (2008). The genome of the model beetle and pest Tribolium castaneum. *Nature* **452**, 949-955.

Roth, S. and Hartenstein, V. (2008). Development of Tribolium castaneum. *Dev. Genes Evol.* **218**, 115-118.

Sarrazin, A. F., Peel, A. D. and Averof, M. (2012). A segmentation clock with two-segment periodicity in insects. *Science* **336**, 338-341.

Schinko, J. B., Kreuzer, N., Offen, N., Posnien, N., Wimmer, E. A. and Bucher, G. (2008). Divergent functions of orthodenticle, empty spiracles and buttonhead in early head patterning of the beetle Tribolium castaneum (Coleoptera). *Dev. Biol.* **317**, 600-613.

Schröder, R., Beermann, A., Wittkopp, N. and Lutz, R. (2008). From development to biodiversity–Tribolium castaneum, an insect model organism for short germband development. *Dev. Genes Evol.* **218**, 119-126.

Stelzer, E. H. K. and Lindek, S. (1994). Fundamental reduction of the observation volume in far-field light microscopy by detection orthogonal to the illumination axis: confocal theta microscopy. *Opt. Commun.* **111**, 536-547.

Tomoyasu, Y. and Denell, R. E. (2004). Larval RNAi in Tribolium (Coleoptera) for analyzing adult development. *Dev. Genes Evol.* **214**, 575-578.

Tomoyasu, Y., Miller, S. C., Tomita, S., Schoppmeier, M., Grossmann, D. and Bucher, G. (2008). Exploring systemic RNA interference in insects: a genome-wide survey for RNAi genes in Tribolium. *Genome Biol.* **9**, R10.

van der Zee, M., Berns, N. and Roth, S. (2005). Distinct functions of the Tribolium zerknüllt genes in serosa specification and dorsal closure. *Curr. Biol.* **15**, 624-636.